Eur. Phys. J. C (2025) 85:1256
https://doi.org/10.1140/epjc/s10052-025-15005-z

THE EUROPEAN PHYSICAL JOURNAL C

Regular Article - Theoretical Physics

Black hole in Dehnen $\left(1, 4, \frac{1}{2}\right)$ dark matter halo: exact solution, lensing, light ring, and thermodynamics

David Senjaya[a]

Department of Physics, Faculty of Science, Mahidol University, Bangkok 10400, Thailand

Received: 14 September 2025 / Accepted: 26 October 2025

Abstract In this work, we present the exact solution of a static, spherically symmetric black hole embedded in a Dehnen $\left(1, 4, \frac{1}{2}\right)$ dark matter halo. We explore both its optical and thermodynamic properties. Using the principle of least action, we derive the null geodesics to analyze and illustrate the corresponding gravitational lensing and light ring phenomena in the presence of the dark matter halo. We then turn to the thermodynamics of the black hole–dark matter system, examining the mass function, entropy, temperature, heat capacity, and Gibbs free energy to assess both local and global stability. Our results show that the surrounding dark matter halo plays a crucial role: it not only enhances the thermodynamic stability of the black hole but also enables the occurrence of phase transitions.

1 Introduction

Einstein's General Relativity (GR) has been tested extensively and confirmed in many regimes, yet it remains incomplete when addressing fundamental issues such as black hole singularities, dark matter, and dark energy. Observations of gravitational waves and black hole shadows by the Event Horizon Telescope [1,2] provide compelling evidence for the existence of black holes, consistent with GR predictions. However, galactic-scale observations reveal discrepancies: the rotation curves of large galaxies remain flat at large radii, a phenomenon that cannot be explained solely by visible matter. This discrepancy gave rise to the dark matter hypothesis, which postulates an invisible mass component that dominates galactic dynamics.

Recent astronomical research continues to strengthen the case for dark matter (DM), showing that the rotational motion of stars in galaxies requires DM to account for up to 90% of the total galactic mass, with baryonic matter comprising only a small fraction. Studies suggest that during the early universe, DM accumulated near galactic centers, fostering star formation, before gradually redistributing to form extended halos as galaxies evolved. Furthermore, current evidence indicates that most massive elliptical and spiral galaxies host central supermassive black holes enveloped by vast DM halos [3]. These findings highlight the importance of investigating black hole solutions embedded in dark matter environments, as they may provide new insights into the interplay between gravity, galactic dynamics, and fundamental physics beyond GR.

Black hole solutions that incorporate realistic dark matter profiles have attracted growing attention in recent years. Several notable works include studies of the Schwarzschild black hole embedded in a Hernquist-type dark matter halo [4], as well as black holes surrounded by different Dehnen profiles such as $(1, 4, 0)$ [5], $(1, 4, 1)$ [6], $(1, 4, 2)$ [7] and $1, 4, \frac{5}{2}$ [8,9] also Dehnen $(1, 4, 1)$ in combination with nonzero cosmological constant [10]. These configurations reveal distinctive physical properties, ranging from thermodynamic behavior to optical signatures such as shadows and gravitational lensing.

On the other hand, thermodynamics and BHs are profoundly intertwined, beginning with the earlier research of Bekenstein and Hawking, when Bekenstein first established a relationship between a black hole's event horizon area and entropy, observing that both rise irreversibly in classical black holes [11]. From a macroscopic perspective, these are extremely basic objects that require only a few parameters to fully characterize [12–16]. In addition to entropy and Hawking temperature [11], the most general black hole is described by a few parameters: mass M, charge Q, and angular momentum J. A black hole thermodynamic description is completed by these variables yielding the establishment

[a] e-mail: davidsenjaya@protonmail.com (corresponding author)

Published online: 05 November 2025

of the four laws of black hole thermodynamics in the 1970s. This new paradigm is known as black hole chemistry [17,18].

Understanding the influence of dark matter halos on black holes is of particular importance for astrophysics. Supermassive black holes residing at galactic centers are naturally embedded in extended dark matter distributions, and the halo structure itself plays a central role in explaining galactic rotation curves. Investigating such black hole–dark matter systems is therefore essential for probing the interplay between compact objects and their environments, and may ultimately shed light on the connection between black hole physics, dark matter phenomenology, and galaxy formation.

In this work, we employ the method developed in [19] to construct a new static, spherically symmetric black hole solution embedded in a Dehnen-type $\left(1, 4, \frac{1}{2}\right)$ dark matter halo. We analyze both the timelike geodesics of test particles and the thermodynamic properties of the black hole–dark matter system. This allows us to gain deeper insight into how the Dehnen-type $\left(1, 4, \frac{1}{2}\right)$ density profile influences particle motion as well as the stability and phase structure of the black hole.

2 Black hole construction

In this work, we focus on the Dehnen-type dark matter halo [20], characterized by the mass density profile,

$$\rho(r) = \rho_0 \left(\frac{r}{r_0}\right)^{-\gamma} \left(1 + \left(\frac{r}{r_0}\right)^{\alpha}\right)^{\frac{\gamma-\beta}{\alpha}}, \tag{1}$$

with $(\alpha, \beta, \gamma) = \left(1, 4, \frac{1}{2}\right)$, which leads to the explicit expression,

$$\rho(r) = \rho_0 \left(\frac{r}{r_0}\right)^{-\frac{3}{2}} \left(1 + \frac{r}{r_0}\right)^{-\frac{7}{2}}, \tag{2}$$

where ρ_0 denotes the central density of the dark matter halo and r_0 is halo core radius [5]. For a spherically symmetric spacetime, the corresponding mass distribution function is given as [21],

$$M_{DM} = \int d\Omega_2 \int_{r'=0}^{r} \rho(r') r'^2 dr' = \frac{8}{5}\pi\rho_0 r_0^3 \left(1 + \frac{r_0}{r}\right)^{-\frac{5}{2}}. \tag{3}$$

The Dehnen $\left(1, 4, \frac{1}{2}\right)$ profile is particularly significant because it represents the minimum inner slope required to establish a self-consistent dark matter distribution around supermassive black holes [22]. Profiles with shallower inner slopes fail to maintain dynamical equilibrium near the black hole, leading to instabilities or mass deficits in the central region. Recent numerical simulations and observational studies indicate that realistic galactic centers, especially in massive elliptical and spiral galaxies, exhibit steep inner density profiles that are well approximated by the Dehnen-type distributions. Moreover, the Dehnen $\left(1, 4, \frac{1}{2}\right)$ profile captures key features of both the central cusp and the outer halo, making it suitable for investigating phenomena such as stellar dynamics, black hole accretion, and gravitational lensing. Its relevance extends to modeling the interplay between supermassive black holes and surrounding dark matter, which is crucial for understanding galactic rotation curves, black hole growth, and the formation of high-density stellar cores.

We now proceed to construct a static, spherically symmetric black hole solution embedded within a dark matter halo. To achieve this, we adopt the following metric ansatz for a static, spherically symmetric spacetime, where the mass distribution of the surrounding halo is described by the Dehnen $\left(1, 4, \frac{1}{2}\right)$ density profile,

$$ds^2 = -h(r)dt^2 + \frac{dr^2}{h(r)} + r^2\left(d\theta^2 + \sin^2\theta d\phi^2\right), \tag{4}$$

$$h(r) = -\frac{r_s}{r} + f(r). \tag{5}$$

Here $r_s = 2M$ denotes the Schwarzschild radius, with M representing the black hole mass. In the absence of the black hole ($r_s = 0$), the spacetime reduces to a pure dark matter background, and the geometry is entirely determined by the halo distribution. In this case, the energy–momentum tensor arises solely from the dark matter halo.

The Einstein field equations for the black hole + dark matter halo is written as,

$$R_{\mu\nu} - \frac{1}{2}Rg_{\mu\nu} = 8\pi T_{\mu\nu}, \tag{6}$$

here, $T_{\mu\nu} = \text{diag}\left[\rho_E, p_r, p, p\right]$ represents the energy–momentum tensor of the black hole + dark matter halo. The independent components of the Einstein field equations for the static, spherically symmetric spacetime are then given by,

$$8\pi T_{tt} = -f\left[\frac{f-1}{r^2} + \frac{\partial_r f}{r}\right], \tag{7}$$

$$8\pi T_{rr} = \frac{1}{f}\left[f\left[\frac{\partial_r f}{rf} + \frac{1}{r^2}\right] - \frac{1}{r^2}\right], \tag{8}$$

$$8\pi T_{\theta\theta} = \frac{r^2}{2}\left[\left\{\partial_r^2 f - \frac{(\partial_r f)^2}{2f} + \frac{\partial_r f}{r}\right\} + \partial_r f\left\{\frac{\partial_r f}{4f} + \frac{1}{2r}\right\}\right]. \tag{9}$$

In a spherically symmetric geometry, the tangential velocity is directly related to the metric function $f(r)$ [19] as the tangential velocity is determined by the enclosed dark matter distribution (3),

$$v_t^2(r) = \frac{M_{DM}(r)}{r} = \frac{8}{5}\pi\rho_0 r_0^3 \sqrt{\frac{r^3}{(r+r_0)^5}} = r\frac{d}{dr}\left(\ln\sqrt{f(r)}\right). \tag{10}$$

Integrating the equation, we obtain $f(r)$,

$$f(r) = e^{2\int \frac{v_t^2(r)}{r}dr}, \\ = e^{\frac{32}{15}\pi\rho_0 r_0^2\sqrt{\left(\frac{r}{r+r_0}\right)^3}}. \tag{11}$$

Accordingly, the explicit form of the static, spherically symmetric black hole metric with a Dehnen $(1, 4, \frac{1}{2})$ dark matter halo is given explicitly by,

$$ds^2 = -\left[e^{\frac{32}{15}\pi\rho_0 r_0^2\sqrt{\left(\frac{r}{r+r_0}\right)^3}} - \frac{r_s}{r}\right]dt^2 + \frac{dr^2}{e^{\frac{32}{15}\pi\rho_0 r_0^2\sqrt{\left(\frac{r}{r+r_0}\right)^3}} - \frac{r_s}{r}} \\ + r^2 d\Omega_2^2. \tag{12}$$

The explicit expression of $T_{\mu\nu} = \text{diag}\,[\rho_E, p_r, p, p]$ can straightforwardly obtained by substituting the obtained metric (12) into Eqs. (7) to (9), yielding,

$$\rho_E = \frac{1}{8\pi r^2}\left[e^{\frac{32}{15}\pi\rho_0 r_0^2\sqrt{\left(\frac{r}{r+r_0}\right)^3}} - \frac{r_s}{r}\right] \\ \times\left[e^{\frac{32}{15}\pi\rho_0 r_0^2\sqrt{\left(\frac{r}{r+r_0}\right)^3}}\left(1 + \frac{16}{5}\pi\rho_0 r_0^3\sqrt{\frac{r^3}{(r+r_0)^5}}\right) - 1\right], \tag{13}$$

$$p_r = \frac{1}{8\pi r^2} \\ \times\left[e^{\frac{32}{15}\pi\rho_0 r_0^2\sqrt{\left(\frac{r}{r+r_0}\right)^3}}\left(1 + \frac{16}{5}\pi\rho_0 r_0^3\sqrt{\frac{r^3}{(r+r_0)^5}}\right) - 1\right], \tag{14}$$

$$p = \frac{1}{1600\pi r(r+r_0)^5\left(e^{\frac{32}{15}\pi\rho_0 r_0^2\sqrt{\left(\frac{r}{r+r_0}\right)^3}} r - r_s\right)} \\ \times\Big[25(r+r_0)^5 r_s^2 + 32\pi r^{7/2}\rho_0 r_0^3 \\ \times\left(24\pi r^{3/2}\rho_0 r_0^3 - 5(r-4r_0)\sqrt{(r+r_0)^3}\right) \\ +2r r_s e^{\frac{32}{15}\pi\rho_0 r_0^2\sqrt{\left(\frac{r}{r+r_0}\right)^3}}\left(400\pi\rho_0 r_0^4\sqrt{r^3(r+r_0)^3}\right. \\ +25r(r^4 + 5r^3 r_0 + 10r r_0^3 + 5r_0^4 \\ \left.+2r^2 r_0^7(125 + 256\pi^2 r_0^4\rho_0^2))\right)\Big], \tag{15}$$

Note that ρ_E denotes the effective energy density appearing in the Einstein field equations $G_{\mu\nu} = R_{\mu\nu} - \frac{1}{2}Rg_{\mu\nu} = 8\pi T_{\mu\nu}$. Hence, $\rho_E \neq \rho$, although they are physically related.

3 Light dynamics

This section focuses on the motion of photons in the spacetime of a Schwarzschild black hole surrounded by a Dehnen $\left(1, 4, \frac{1}{2}\right)$ dark matter halo described by the metric (12). We first write down the Lagrangian for the massless particle as follows,

$$L(x^\alpha, \dot{x}^\alpha) = \frac{1}{2}g_{\mu\nu}\dot{x}^\mu\dot{x}^\nu = \frac{1}{2}\left[-h(r)\dot{t}^2 + \frac{\dot{r}^2}{h(r)} + r^2\dot{\theta}^2 \right. \\ \left. + r^2\sin^2\theta\dot{\phi}^2\right] = 0. \tag{16}$$

Clearly, the Lagrangian (16) does not explicitly depend on t and ϕ. The corresponding conserved quantities along these directions are constants of motion, i.e. the photon's energy E and angular momentum L,

$$p_t = \frac{\partial L}{\partial \dot{t}} = -h(r)\dot{t} = -E, \tag{17}$$

$$p_\phi = \frac{\partial L}{\partial \dot{\phi}} = r^2\dot{\phi}\sin^2\theta = L. \tag{18}$$

For a spherically symmetric spacetime, the motion of particles or photons can always be confined to a plane due to the spherical symmetry of the metric. Without loss of generality, we choose the equatorial plane $\theta = \frac{\pi}{2}$, which simplifies the analysis while preserving the generality of the results. In this plane, the Lagrangian (16) reduces to a simpler form, as the θ-dependent terms vanish, allowing us to focus solely on the radial and azimuthal dynamics of the photon. This simplification is standard in studies of black hole geodesics and facilitates the derivation of conserved quantities and effective potentials.

In the equatorial plan, the Lagrangian (16) simplifies to,

$$L(r, \dot{t}, \dot{r}, \dot{\phi}) = \frac{1}{2}\left[-h(r)\dot{t}^2 + \frac{\dot{r}^2}{h(r)} + r^2\dot{\phi}^2\right] \\ = \frac{1}{2}\left[-\frac{E^2}{h(r)} + \frac{\dot{r}^2}{h(r)} + \frac{L^2}{r^2}\right] = 0. \tag{19}$$

and this reduction highlights that the dynamics of the photon are fully described by its radial and azimuthal motion, with the conserved energy E and angular momentum L governing the trajectory.

We now proceed to derive the radial equation of motion,

$$\dot{r}^2 + \frac{L^2}{r^2}h(r) = E^2, \tag{20}$$

where the first term on the left-hand side represents the radial kinetic energy of the photon, and the second term defines the effective potential V_{eff}. Explicitly, the effective potential is given by,

$$V_{eff} = \frac{L^2}{r^2}h(r) = \frac{L^2}{r^2}\left[e^{\frac{32}{15}\pi\rho_0 r_0^2\sqrt{\left(\frac{r}{r+r_0}\right)^3}} - \frac{r_s}{r}\right]. \tag{21}$$

Figure 1 illustrates the behavior of the effective potential V_{eff} for photons around a Schwarzschild black hole embedded in a Dehnen $\left(1, 4, \frac{3}{2}\right)$ dark matter halo, for various combinations of black hole and halo parameters. Each curve cor-

responds to different choices of the halo central density ρ_0, core radius r_0 and angular momentum L. The plot shows that the peak of the effective potential, which determines the location of the photon sphere, increases with larger angular momentum and larger halo parameters ρ_0 and r_0.

Next, we examine the equatorial circular orbits of photons around a static, spherically symmetric black hole embedded in the dark matter. On the equatorial plane, circular orbits, where the condition $\dot{r} = 0$ is satisfied, occur at the maxima of the effective potential $V'_{eff} = 0$, where the radial force on the photon vanishes. Applying the equation of motion (20) under the condition $\dot{r} = 0$ yields,

$$V_{eff} = \frac{L^2}{r^2}\left[e^{\frac{32}{15}\pi\rho_0 r_0^2\sqrt{\left(\frac{r}{r+r_0}\right)^3}} - \frac{r_s}{r}\right] = E^2. \tag{22}$$

while at the maxima of the effective potential,

$$V'_{eff} = 15r_s + 2e^{\frac{32}{15}\pi\rho_0 r_0^2\sqrt{\left(\frac{r}{r+r_0}\right)^3}} r \times \left(8\pi\rho_0 r_0^3\sqrt{\frac{r^3}{(r+r_0)^5}} - 5\right) = 0. \tag{23}$$

Eliminating the exponential term in (23) using (22), we obtain the following simplified relation,

$$15r_s + 2\left(\frac{E^2 r^3}{L^2} + r_s\right)\left(8\pi\rho_0 r_0^3\sqrt{\frac{r^3}{(r+r_0)^5}} - 5\right) = 0, \tag{24}$$

The above relation can be expressed as a series expansion in the parameter r_0, resulting in the following quartic equation,

$$q(r_c) \equiv -10\left(r_c^4 - \left[\frac{8}{5}\pi\rho_0 r_0^3\right]r_c^3\left[\frac{r_s b^2}{2}\right]r_c - \left[\frac{8}{5}\pi b^2\rho_0 r_0^3\right]\right) = 0, \tag{25}$$

where r_c denotes the radius of the photon circular orbit, and the ratio $b = \frac{L}{E}$ is the photon's impact parameter.

Figure 2 shows the profile of the quartic equation ((25)). We graph $q(r_c)$ for several combinations of black hole parameters and impact parameter values. Notice that $q(r_c)$ has a single zero at $r_c > 0$ for the given parameter combination.

In Fig. 3, we plot the function $q(r_c)$ for the parameters $\rho_0 = 0.001$, $r_0 = 0.5$, $r_s = 1$, and $L = 1$. The figure clearly demonstrates that each $q(r_c)$ curve intersects the r-axis at exactly one point, indicating that every function possesses a single zero. This intersection corresponds to the radius of the circular photon orbit for the given energy and angular momentum. Notably, for a fixed angular momentum, decreasing the photon energy shifts the circular orbit to larger radii. This behavior is consistent with analytical predictions, where photons with very low energy – corresponding to extremely large impact parameters – fail to intersect the r-axis entirely, implying the absence of a stable circular orbit. Additionally, the figure highlights how the orbital radius varies smoothly with photon energy, illustrating the continuous dependence of the circular orbit on the impact parameter and providing insight into photon dynamics around the black hole.

3.1 The light ring

Let us now reconsider eq.(20). By making use of the relation,

$$\dot{r} = \frac{dr}{d\phi}\dot{\phi}, \tag{26}$$

together with the definition of the impact parameter,

$$\frac{1}{b} = \frac{E}{L} = \frac{h(r)}{r^2\frac{d\phi}{dt}}. \tag{27}$$

Substituting these expressions into (20) leads to,

$$\left(\frac{dr}{d\phi}\right)^2 = \frac{r^4}{L^2}\left(E^2 - \frac{L^2}{r^2}h(r)\right) = \frac{r^4}{b^2} - r^2 h(r) = r^2 h(r)\left(\frac{r^2}{b^2 h(r)} - 1\right). \tag{28}$$

Now, let us consider the following set of conditions that define the photon sphere. In this case, the trajectory of light is governed by the equations,

$$\frac{dr}{d\phi} = \frac{d^2 r}{d\phi^2} = 0. \tag{29}$$

Explicitly, these conditions lead to,

$$\frac{dr}{d\phi} = 0 \rightarrow \frac{r^2}{b^2 h(r)} = 1, \tag{30}$$

$$\frac{d^2 r}{d\phi^2} = 0 \rightarrow \frac{d}{dr}\left(\frac{r^2}{h(r)}\right) = 0. \tag{31}$$

Equations Eqs. (30) and (31) together ensure that the net radial force acting on the photon vanishes, thereby allowing the photon to remain stationary in a fixed circular orbit at radius r. In particular, the condition (31) corresponds to the requirement that the effective potential has an extremum at this location. Explicitly, the zero-force equation can be written as,

$$2rh(r) - r^2 h'(r) = 0. \tag{32}$$

Substituting $h(r)$ into the photon sphere conditions, we obtain,

$$-3r_s + \frac{2}{5}e^{\frac{32}{15}\pi\rho_0 r_0^2\sqrt{\left(\frac{r}{r+r_0}\right)^3}} r\left[1 - 8\pi\rho_0 r_0^3\sqrt{\frac{r^3}{(r+r_0)^5}}\right] = 0, \tag{33}$$

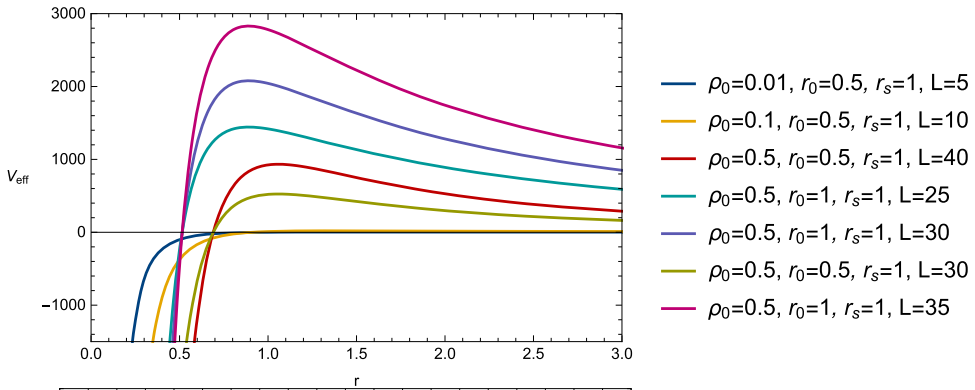

Fig. 1 Profile of effective potential for various black holes in Dehnen $\left(1, 4, \frac{3}{2}\right)$ dark matter halo

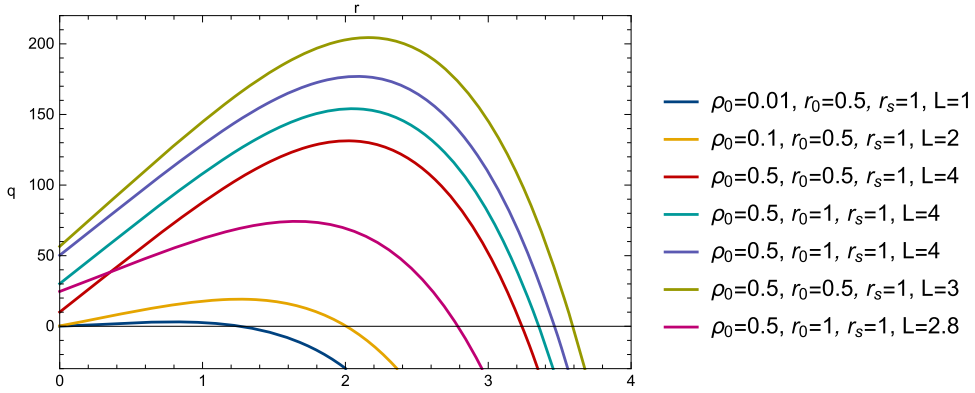

Fig. 2 Profile of $q(r_c)$ for selected various dark matter parameter

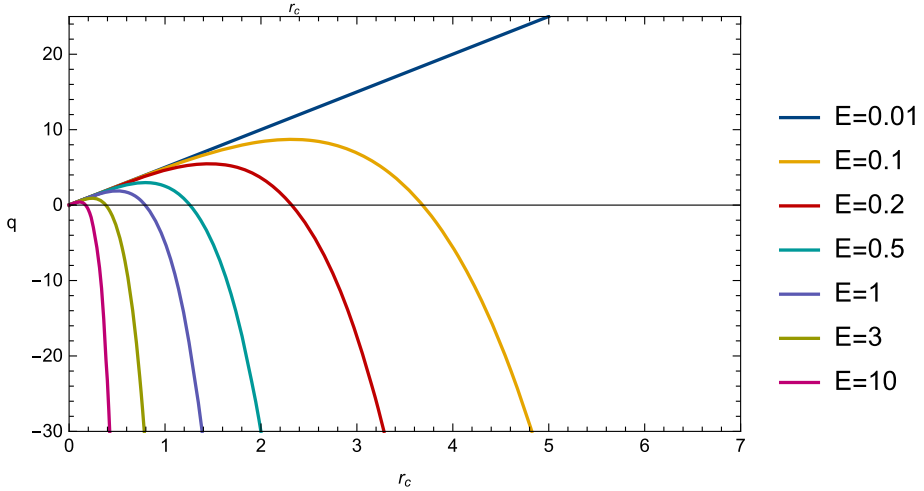

Fig. 3 Profile of $q(r_c)$ for various energy with fixed $\rho_0 = 0.001, r_0 = 0.5, r_s = 1, L = 1$

whose solution, $r = r_{ps}$, corresponds to the location of the so-called photon sphere. This radius marks the critical circular null orbit and therefore determines the edge of the black hole shadow as seen by a distant observer.

It is instructive to check the limiting case in which the dark matter density vanishes, $\rho_0 = 0$. In this limit, equation (33) simplifies to,

$$-3r_s + 2r = 0, \tag{34}$$

with the solution $r = r_{ps} = \frac{3}{2}r_s$ which exactly reproduces the well-known Schwarzschild photon sphere. This consistency confirms that the generalized condition smoothly reduces to the standard vacuum result in the absence of dark matter.

Using the condition (30), the critical impact parameter b_c is obtained as,

$$\frac{1}{b_c} = \sqrt{\frac{h(r_{ps})}{r_{ps}^2}}. \tag{35}$$

This parameter defines the threshold between photon trajectories that are scattered back to infinity and those that are captured by the black hole. Photons with an impact parameter $b < b_c$ inevitably cross the photon sphere and fall into the black hole, while those with

$$b > b_c$$

will eventually escape to infinity. Thus, b_c effectively characterizes the "size" of the photon sphere as seen from infinity.

In turn, the black hole shadow radius can be defined in terms of the critical impact parameter. Following [23], the shadow radius observed at infinity is,

$$R = b_c\sqrt{h(r\to\infty)} \approx \sqrt{\frac{r_{ps}^2}{h(r_{ps})}e^{\frac{32}{15}\pi\rho_0 r_0^2}}. \tag{36}$$

Figure 4 illustrates the profiles of the shadow radius R for different combinations of the dark matter halo parameters $\{\rho_0, r_0\}$ with a fixed Schwarzschild radius $r_s = 1$. The left panel shows the variation of the apparent photon rings as ρ_0 increases for a fixed $r_0 = 2$. It can be clearly seen that a larger dark matter density shifts the photon ring outward, enlarging the shadow. On the other hand, the right panel demonstrates the effect of varying the scale radius r_0 at a fixed $\rho_0 = 0.001$. In this case, increasing r_0 causes the photon ring to expand. So, in general, black holes with larger $\{\rho_0, r_0\}$ will have larger photon ring.

We may estimate the photon sphere radius by doing a series expansion of equation (33) for the exceptional situation when the dark matter contribution is tiny, i.e., when $\rho_0 r_0^3 \ll 1$. This results in,

$$r_{ps} \approx \frac{9(5r_s + 16\pi\rho_0 r_0^3)}{2(15 + 32\pi\rho_0 r_0^2)}, \tag{37}$$

yielding,

$$R_s \approx \frac{\sqrt{3}}{10}\left[15r_s + 16\pi\rho_0 r_0^3\left(3 + 7\frac{r_s}{r_0}\right)\right]. \tag{38}$$

In the limit where the dark matter contribution vanishes, the above expression reduces to the familiar Schwarzschild result,

$$R_s = \frac{3\sqrt{3}}{2}r_s, \tag{39}$$

which agrees with the standard photon sphere analysis given in [24].

3.2 Weak gravitational lensing

This subsection is devoted to the study of the deflection angle of particles in a static black hole spacetime surrounded by a Dehnen-type dark matter halo characterized by the parameters $\left(1, 4, \frac{1}{2}\right)$. To evaluate the weak-field deflection angle, we employ the Gauss–Bonnet theorem applied to the corresponding optical metric, following the Gibbons–Werner method [25,26]. This geometric approach provides an elegant and powerful way to calculate the deflection angle by relating it to the global topology of the spacetime, rather than relying solely on solving geodesic equations. Other calculation method via the elliptic integral can be found in [27,28].

The deflection angle α can be computed using the Gauss–Bonnet theorem in the weak-field limit, which gives the following integral expression [29],

$$\alpha = \int_{\phi=0}^{\pi}\int_{r=\frac{b}{\sin\phi}}^{\infty} K\sqrt{g_{opt}}\,dr\,d\phi, \tag{40}$$

where K denotes the Gaussian curvature of the optical manifold and g_{opt} is the determinant of the two-dimensional optical metric. The optical metric associated with the line element is given by,

$$dt^2 = \frac{dr^2}{h^2(r)} + \frac{r^2 d\phi^2}{h(r)}, \tag{41}$$

from which we obtain,

$$g_{opt} = \frac{r^2}{h^3(r)}. \tag{42}$$

The Gaussian curvature of this optical geometry is calculated as,

$$K = \frac{1}{2}\left[\frac{1}{2}\left(\frac{dh(r)}{dr}\right)^2 - h(r)\frac{d^2h(r)}{dr^2}\right]. \tag{43}$$

Using (12), we can write the integrand explicitly as a series up to $O(\rho r_0^3)$ as follows,

$$K\sqrt{g_{opt}} \approx \frac{(4r - 3r_s)r_s}{4\sqrt{(r(r-r_s))^3}} - \frac{4\pi r_s\rho_0 r_0^2(r_s - 4r)}{15\sqrt{r(r-r_s)^5}} + \frac{2\pi\rho r_0^3(8r^2 - 8rr_s + 3r_s^2)}{5\sqrt{r^3(r-r_s)^5}}, \tag{44}$$

which leads to,

$$\alpha \approx \frac{2}{15b}\left[(15 - 16\pi r_0^2)r_s + 5\rho_0\pi r_0^3(16 + 3\pi b^{-1}r_s)\right]. \tag{45}$$

Observe that $\alpha = 2b^{-1}r_s$, the deflection angle of the pure Schwarzschild black hole, is obtained if $\rho_0 = r_0 = 0$ [26].

Figure 5 shows the deflection angle for various r_0 values. This graphic depicts the gravitational deflection angle as a function of the impact parameter for black holes surrounded by Dehnen $\left(1, 4, \frac{1}{2}\right)$ dark matter, with black hole mass $r_s = 1$ and $\rho_0 = 0.001$. The study found that at low impact parameters $b \ll 1$, the deflection angle rises, suggesting a substantial gravitational lensing effect. As the impact parameter increases, $b \gg 1$, the deflection angle decreases and eventually approaches zero, as predicted.

4 Black hole thermodynamics

The thermodynamics of a Schwarzschild black hole submerged in Dehnen $\left(1, 4, \frac{1}{2}\right)$ dark matter is explored in this

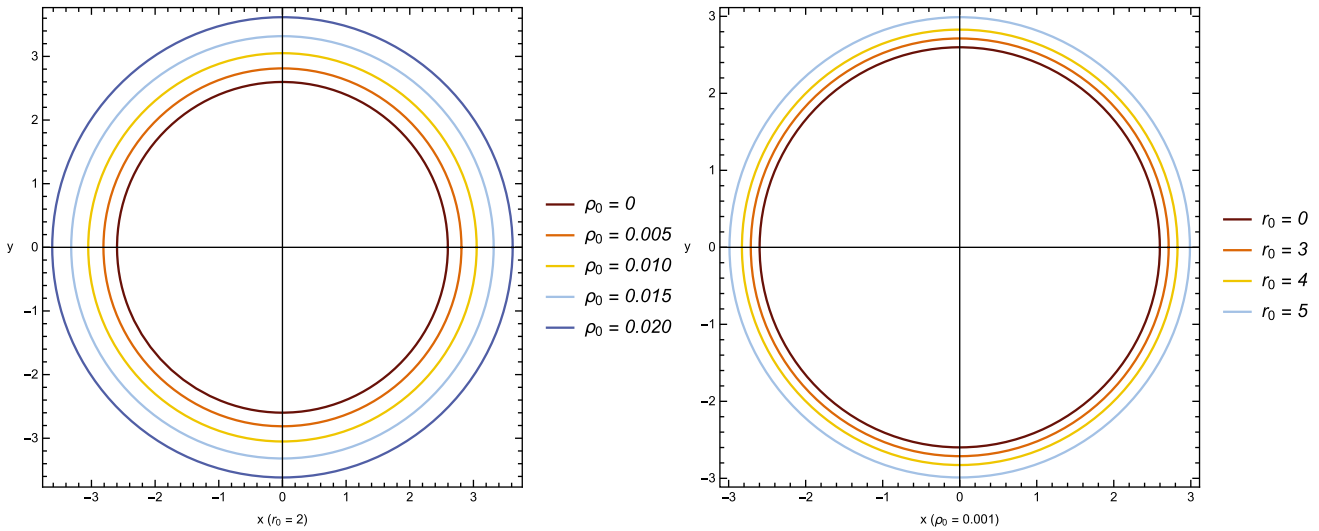

Fig. 4 Profile of R for various combinations of $\{\rho_0, r_0\}$ with $r_s = 1$

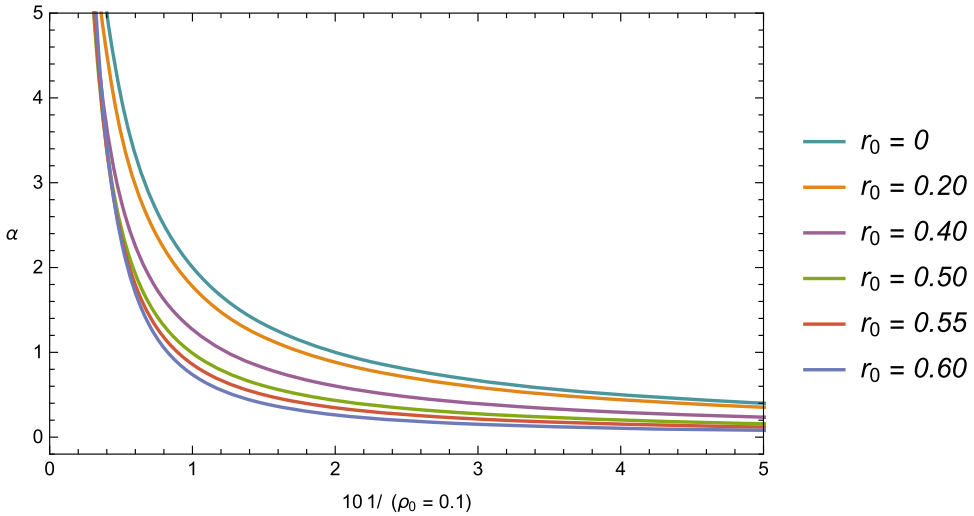

Fig. 5 Profile of α for various combinations of $\{\rho_0 = 001, r_0\}$ with $r_s = 1$

section. We start by looking at the horizon position r_H, which can be found using $g_{tt} = 0$, yielding,

$$M = \frac{r_H}{2} e^{\frac{32}{15}\pi\rho_0 r_0^2\sqrt{\left(\frac{r}{r+r_0}\right)^3}}. \tag{46}$$

In the framework of black hole thermodynamics, the thermodynamic enthalpy analogous to classical thermodynamics corresponds precisely to the mass M, as defined by (46) [30,31]. The Hawking temperature is determined by the surface gravity at the event horizon, expressed mathematically as,

$$T = \frac{f'(r_H)}{4\pi} = e^{\frac{32}{15}\pi\rho_0 r_0^2\sqrt{\left(\frac{r}{r+r_0}\right)^3}}\left[\frac{1}{4\pi r_H} + \frac{4}{5}\rho_0 r_0^3\sqrt{\frac{r_H}{(r_0+r_H)^5}}\right]. \tag{47}$$

For different combinations of $\{\rho_0, r_0\}$, the black hole's temperature T with respect to r_H is displayed in Fig. 6. The behavior of T with fixed $r_0 = 2$ ($\rho_0 = 0.01$) is depicted in the upper (lower) graph. For configurations with not zero $\{\rho_0, r_0\}$, there are two distinct phases, i.e. positive slope regions, with $\frac{\partial T}{\partial r_H} > 0$, and negative slope regions, with $\frac{\partial T}{\partial r_H} < 0$. The signature of their heat capacities must be investigated in order to assess the stability of each branch.

Moreover, according to [5], the horizon area law defines the black hole's entropy as follows,

$$S = \int \frac{1}{T}\frac{dM}{dr_H} dr_H = \frac{A}{4} = \pi r_H^2, \tag{48}$$

which is positive and continuous for $r_H > 0$.

A black hole's heat capacity must be determined in order to determine its thermal stability as a thermodynamic system. Since the system absorbs energy as its temperature rises, a positive heat capacity denotes thermodynamic stability and

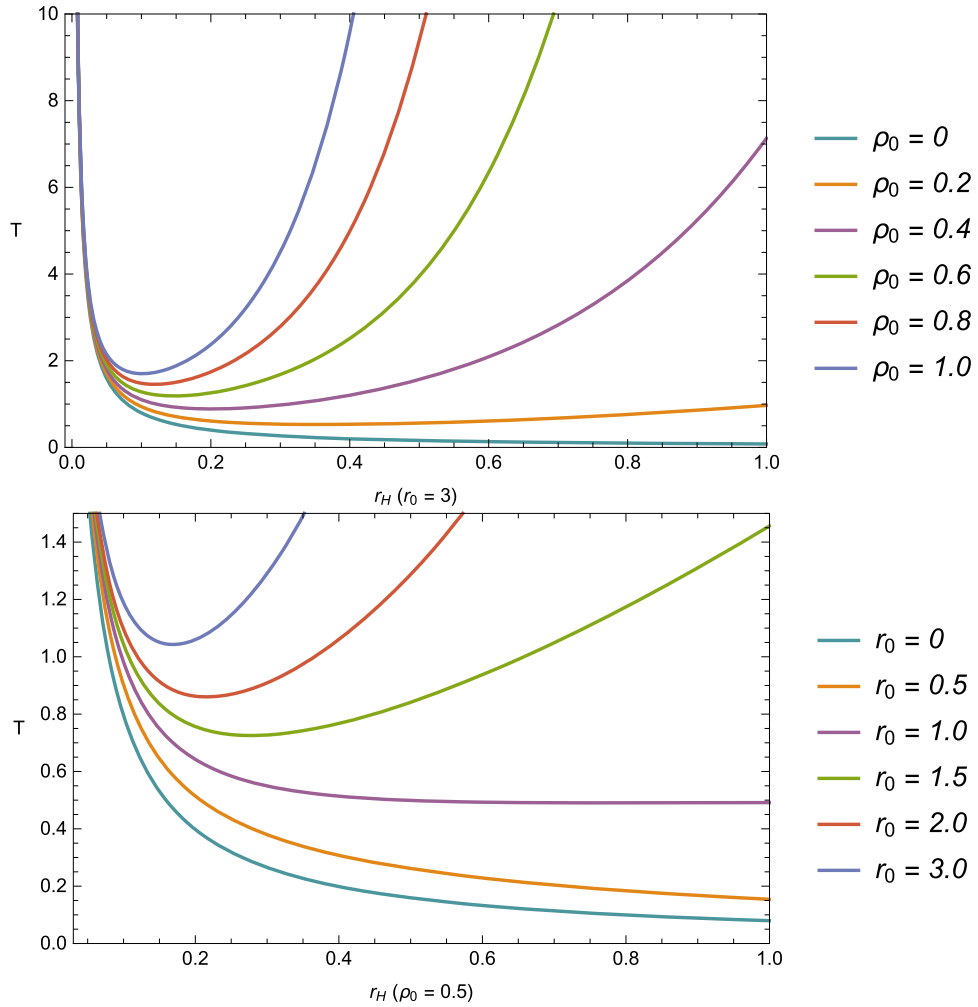

Fig. 6 Profile of T as function of r_H for various $\{\rho_0, r_0\}$

is consistent with standard thermodynamic behavior. A negative heat capacity, on the other hand, indicates an unstable configuration in which the system paradoxically cools when it absorbs heat [18,32].

The specific heat capacity of the static, spherically symmetric black hole embedded in a Dehnen $\left(1, 4, \frac{1}{2}\right)$ dark matter halo is derived as follows,

the Schwarzschild black hole is stabilized by the Dehnen $\left(1, 4, \frac{1}{2}\right)$ dark matter halo. It should be mentioned that larger ρ_0 and r_0 decrease the negative area of the heat capacity.

Additionally, it is crucial to stress that the C_H curves break at the minimum point of $T(r_H)$, i.e. when $\frac{\partial T}{\partial r_H} = 0$, and it is simple to see that the stable (unstable) branch with $C_H > 0 (< 0)$ corresponds to the portion of the temperature function

$$C_H = \frac{\partial M}{\partial T} = \frac{\frac{\partial M}{\partial r_H}}{\frac{\partial T}{\partial r_H}} = -\frac{10\pi r_H^2 (r_0 + r_H)^2 \left\{5(r_0 + r_H)^3 + 16\pi\rho_0 r_0^3 \sqrt{r_H^3 (r_0 + r_H)}\right\}}{25(r_0 + r_H)^5 - 256\pi^2 \rho_0^2 r_0^6 r_H^3 - 40\pi\rho_0 r_0^3 (3r_0 - 2r_H)\sqrt{r_H^3 (r_0 + r_H)^3}}. \tag{49}$$

Figure 7 shows the black hole's heat capacity C_H in relation to r_H for various combinations of $\{\rho_0, r_0\}$. The top (lower) graph shows how T behaves with fixed $r_0 = 2$ ($\rho_0 = 0.1$). In fact, the instability of asymptotically flat black holes in the classical ensemble is highlighted by the negative heat capacity of a pure Schwarzschild black hole without dark matter halo $\rho = 0$ [33]. The curves of C_H, which have positive values and are thermodynamically stable, show that that has a positive (negative) slope. Black hole + dark matter configurations without inflection point, i.e. with very small ρ_0, do not have thermodynamically stable branch.

To evaluate the overall stability of the black hole-dark matter system, we investigate the Gibbs free energy G. A positive G indicates global instability in the thermodynamic

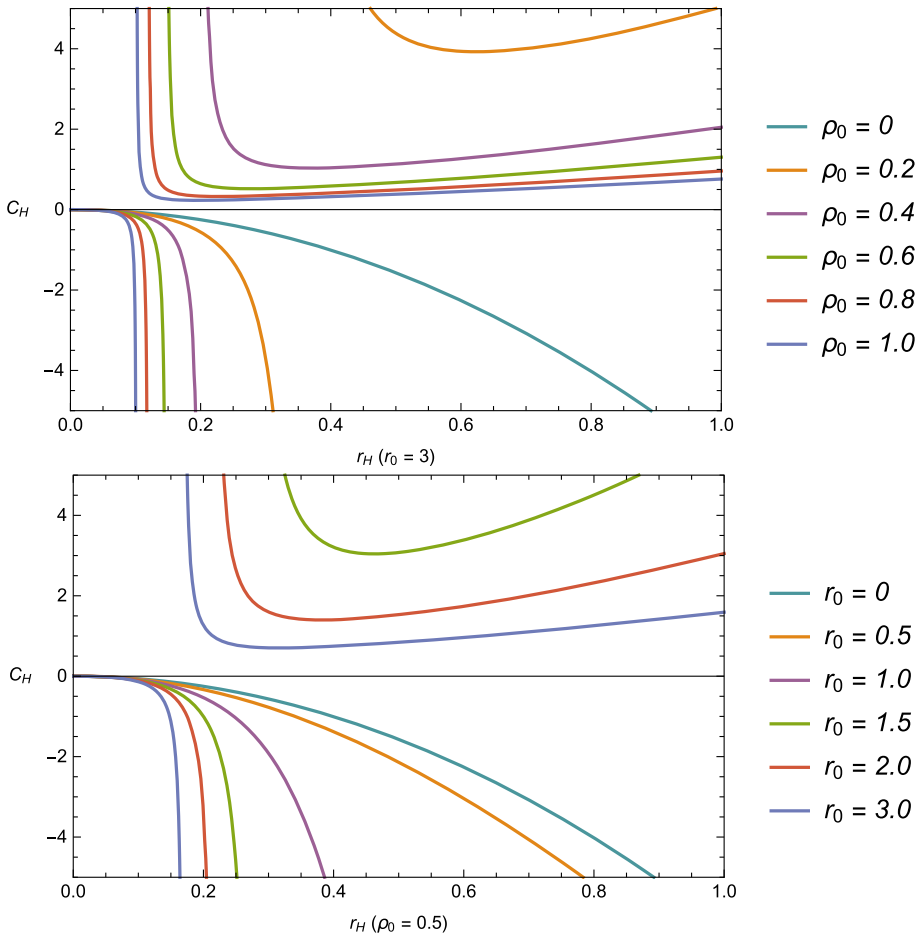

Fig. 7 Profile of C_H as function of r_H for various $\{\rho_0, r_0\}$

system, while a negative value indicates stability. The Gibbs free energy is obtained as,

$$G = M - TS = e^{\frac{32}{15}\pi\rho_0 r_0^2\sqrt{\left(\frac{r}{r+r_0}\right)^3}} r_H \left[\frac{1}{4} - \frac{4}{5}\pi\rho_0 r_0^3\sqrt{\frac{r_H^3}{(r_H+r_0)^5}}\right]. \tag{50}$$

Figure 8 displays the black hole's Gibbs free energy G as a function of r_H for different combinations of $\{\rho_0, r_0\}$. The upper (lower) graph depicts how T behaves with a fixed $r_0 = 2$ ($\rho_0 = 0.04$). Our results show that as core density and halo radius rise, so does the negative area of Gibbs free energy. Both plots show that the presence of a dark matter halo boosts the black hole's global stability.

Figure 9 depict the Gibbs free energy, entropy, and heat capacity as functions of temperature with a fixed $r_0 = 2$. We observe that at critical points, where,

$$\frac{\partial G(T)}{\partial T} = \frac{\partial^2 G(T)}{\partial T^2} = 0 \tag{51}$$

there are these following important observations at the critical temperature: the curvature $\frac{\partial^2 G(T)}{\partial T^2}$ is not continuous even though the Gibbs function $G(T)$ and its slope $\frac{\partial G(T)}{\partial T}$ are continuous. The heat capacity at critical temperature is discontinuous, although entropy is continuous for all temperature levels. It is interesting to observe the behavior the the entropy. The phase transition occurs at the inflection point, where $\frac{\partial S}{\partial T} = \infty$. As a result, configurations without this inflection point cannot undergo phase transition.

Although the Gibbs free energy curve may, at first glance, suggest a possible discontinuity or swallow-tail-like behavior for certain values of $\{\rho_0, r_0\}$, a closer examination reveals that the entropy remains continuous across the transition and no latent heat is released. The absence of any entropy discontinuity excludes the possibility of a first-order phase transition. Instead, the heat capacity diverges at the critical point, indicating an infinite response of the system to infinitesimal temperature fluctuations. According to Ehrenfest's criteria, such behavior characterizes a second-order phase transition, where the first derivatives of the Gibbs free energy are continuous, but the second derivatives become singular. Therefore, despite the apparent shape of the Gibbs free energy curve, the transition in this black hole system is conclusively identified as second order. Also note that, only if ρ_0 is zero does phase transition not occur. A Schwarzschild black hole cannot experience a phase transition.

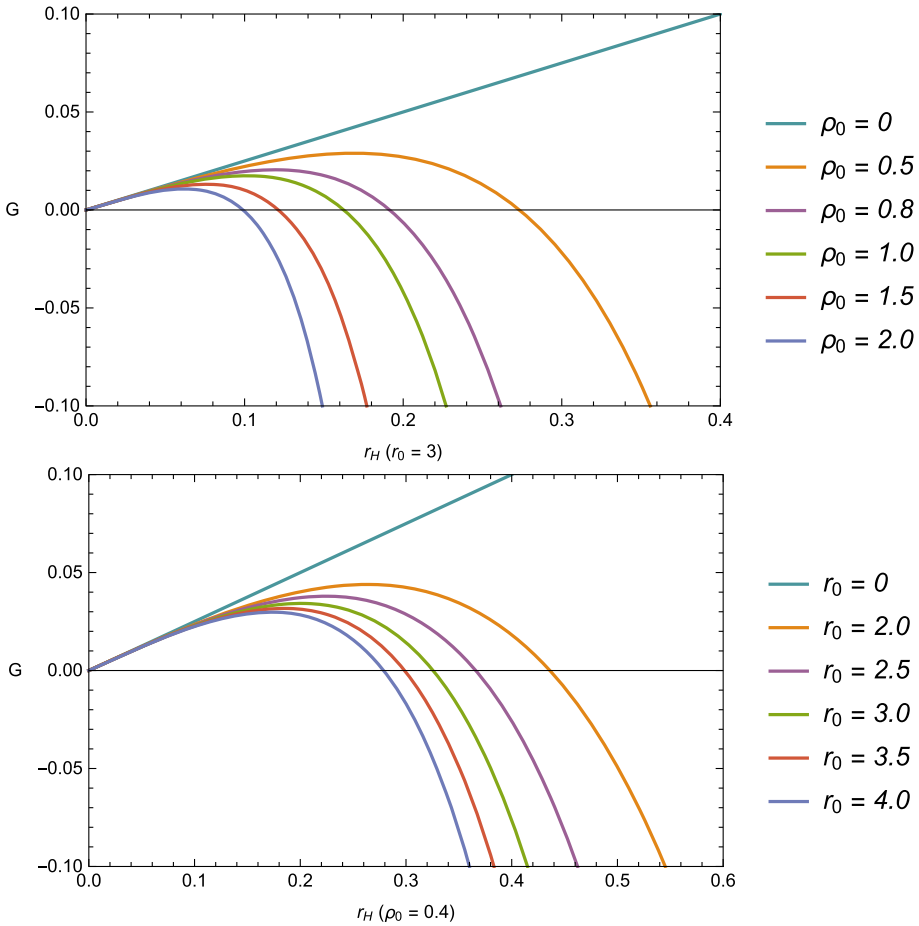

Fig. 8 Profile of G as function of r_H for various $\{\rho_0, r_0\}$

5 Conclusion

In this work, we present an exact static, spherically symmetric black hole solution embedded in a Dehnen $\left(1, 4, \frac{1}{2}\right)$ dark matter halo. Motivated by astrophysical evidence that supermassive black holes reside within extended dark matter distributions, we investigate how such halos influence both the optical and thermodynamic properties of black holes. By deriving null geodesics from the principle of least action, we study photon motion, gravitational lensing, and the formation of light rings, which are central to understanding black hole shadows. In parallel, we examine the thermodynamic behavior of the system by analyzing quantities such as mass, temperature, entropy, heat capacity, and Gibbs free energy.

Our analysis of photon dynamics reveals that the presence of the halo significantly alters the effective potential and the location of the photon sphere. The radius of the photon sphere and the corresponding critical impact parameter increase with larger halo parameters, leading to an enlarged shadow size. Similarly, weak gravitational lensing is enhanced at low impact parameters due to the halo contribution, while asymptotic behavior reduces to the Schwarzschild case when the halo density vanishes. These findings indicate that dark matter imprints distinctive optical signatures on black holes, potentially observable through astrophysical measurements of shadows and lensing.

On the thermodynamic side, we find that the Dehnen halo introduces remarkable differences compared to the pure Schwarzschild case. While Schwarzschild black holes in asymptotically flat space are thermodynamically unstable due to their negative heat capacity, the halo contributes to stabilizing the system. Depending on the values of the halo parameters, the black hole can exhibit locally stable phases with positive heat capacity, as well as globally stable configurations characterized by negative Gibbs free energy. Moreover, the presence of the halo enables phase transitions, a feature absent in the vacuum Schwarzschild black hole. These results highlight the critical role of the dark matter environment in governing black hole thermodynamics.

In conclusion, this study demonstrates that embedding a black hole in a Dehnen $\left(1, 4, \frac{1}{2}\right)$ dark matter halo significantly modifies both its optical and thermodynamic properties. The halo not only alters the photon sphere and shadow but also enhances thermal stability and allows for phase transitions. These findings strengthen the connection between black hole physics and galactic dynamics, suggesting that observational features such as black hole shadows and thermodynamic stability may encode valuable information about

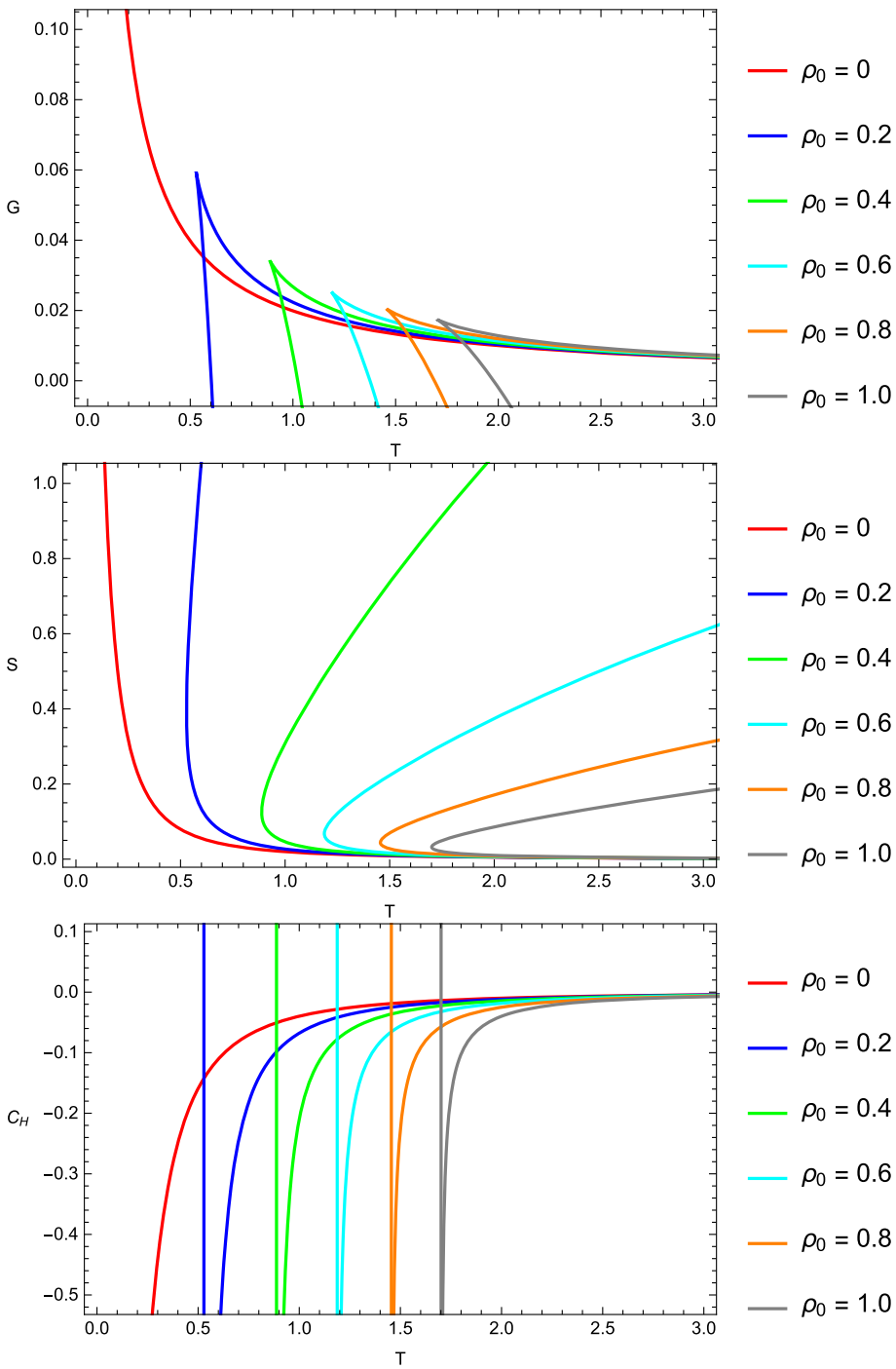

Fig. 9 Profile of $G(T)$, $S(T)$ and $C_H(T)$ for various $\{\rho_0, r_0 = 2\}$

the surrounding dark matter distribution. Future extensions may include exploring rotating (Anti)-de Sitter version to further deepen the link between dark matter and black hole phenomenology.

Data Availability Statement This manuscript has no associated data. [Author's comment: This work is purely theoretical and does not involve any experimental data. Therefore, no datasets were generated or analyzed.].

Code Availability Statement This manuscript has no associated code/software. [Author's comment: This work is purely analytical and does not involve any extraordinary computational code. Hence, no code is available for sharing.].

Funded by SCOAP[3].

References

1. B.P. Abbott et al., Properties of the binary black hole merger GW150914. Phys. Rev. Lett. **116**(24), 241102 (2016). https://doi.org/10.1103/PhysRevLett.116.241102. arXiv:1602.03840 [gr-qc]
2. K. Akiyama et al., First M87 Event Horizon Telescope Results. VI. The shadow and mass of the central black hole. Astrophys. J. Lett. **875**(1), 6 (2019). https://doi.org/10.3847/2041-8213/ab1141
3. S. Rani, A. Jawad, M. Heydari-Fard, U. Zafar, Thermodynamic and shadow analysis of Dehnen type dark matter Halo corrected Schwarzschild black hole surrounded by thin disk. Eur. Phys. J. C **85**(6), 677 (2025). https://doi.org/10.1140/epjc/s10052-025-14388-3
4. S.K. Jha, Thermodynamics, weak gravitational lensing, and parameter estimation of a Schwarzschild black hole immersed in Hernquist dark matter halo. JCAP **06**, 033 (2025). https://doi.org/10.1088/1475-7516/2025/06/033. arXiv:2503.19938 [gr-qc]
5. M.M. Gohain, P. Phukon, K. Bhuyan, Thermodynamics and null geodesics of a Schwarzschild black hole surrounded by a Dehnen type dark matter halo. Phys. Dark Univ. **46**, 101683 (2024). https://doi.org/10.1016/j.dark.2024.101683. arXiv:2407.02872 [gr-qc]
6. B. Toshmatov, B. Ahmedov, A. Boydedayev, B. Ahmedov, Dynamics of black hole in dark matter halo: Quasinormal modes. Phys. Rev. D **111**(12), 124058 (2025). https://doi.org/10.1103/mphy-svrk
7. U. Uktamov, S. Shaymatov, B. Ahmedov, Static black hole solution with a dark matter halo (2025). arXiv:2505.20031 [gr-qc]
8. A. Al-Badawi, S. Shaymatov, Y. Sekhmani, Schwarzschild black hole in galaxies surrounded by a dark matter halo. JCAP **02**, 014 (2025). https://doi.org/10.1088/1475-7516/2025/02/014. arXiv:2411.01145 [gr-qc]
9. F. Hosseinifar, S. Mamedov, F. Studnička, H. Hassanabadi, Quasinormal modes and topological characteristics of a Schwarzschild black hole surrounded by the Dehnen type dark matter halo. Eur. Phys. J. C **85**(8), 819 (2025). https://doi.org/10.1140/epjc/s10052-025-14549-4. arXiv:2503.03260 [gr-qc]
10. F. Ahmed, A. Al-Badawi, İ Sakallı, Observable signatures of black hole with Hernquist dark matter halo having a cloud of strings: geodesic, perturbations, and shadow. Eur. Phys. J. C **85**(9), 984 (2025). https://doi.org/10.1140/epjc/s10052-025-14723-8. arXiv:2506.18457 [gr-qc]
11. S.W. Hawking, Black holes and thermodynamics. Phys. Rev. D **13**, 191–197 (1976). https://doi.org/10.1103/PhysRevD.13.191
12. W. Israel, Event horizons in static vacuum space-times. Phys. Rev. **164**, 1776–1779 (1967). https://doi.org/10.1103/PhysRev.164.1776
13. B. Carter, Axisymmetric black hole has only two degrees of freedom. Phys. Rev. Lett. **26**, 331–333 (1971). https://doi.org/10.1103/PhysRevLett.26.331
14. J.D. Bekenstein, Black holes and the second law. Lett. Nuovo Cim. **4**, 737–740 (1972). https://doi.org/10.1007/BF02757029
15. J.D. Bekenstein, Black holes and entropy. Phys. Rev. D **7**, 2333–2346 (1973). https://doi.org/10.1103/PhysRevD.7.2333
16. R.N. Izmailov, E.R. Zhdanov, A. Bhadra, K.K. Nandi, Relative time delay in a spinning black hole as a diagnostic for no-hair theorem. Eur. Phys. J. C **79**(2), 105 (2019). https://doi.org/10.1140/epjc/s10052-019-6618-6
17. R.B. Mann, Recent developments in holographic black hole chemistry. JHAP **4**(1), 1–26 (2024). https://doi.org/10.22128/jhap.2023.757.1067. arXiv:2403.02864 [hep-th]
18. R.B. Mann, Black hole chemistry: the first 15 years. Int. J. Mod. Phys. D **34**(09), 2542001 (2025). https://doi.org/10.1142/S0218271825420015
19. Z. Xu, X. Hou, X. Gong, J. Wang, Black hole space-time in dark matter halo. JCAP **09**, 038 (2018). https://doi.org/10.1088/1475-7516/2018/09/038. arXiv:1803.00767 [gr-qc]
20. W. Dehnen, A family of potential–density pairs for spherical galaxies and bulges. Mon. Not. R. Astron. Soc. **265**(1), 250–256 (1993). https://doi.org/10.1093/mnras/265.1.250
21. H. Mo, F. Bosch, S. White, *Galaxy Formation and Evolution* (Cambridge University Press, Cambridge, 2010)
22. M. Arca-Sedda, B. Kocsis, T.D. Brandt, Gamma-ray and X-ray emission from the galactic centre: hints on the nuclear star cluster formation history. Mon. Not. R. Astron. Soc. **479**(1), 900–916 (2018). https://doi.org/10.1093/mnras/sty1454. https://arxiv.org/abs/https://academic.oup.com/mnras/article-pdf/479/1/900/25139601/sty1454.pdf. https://academic.oup.com/mnras/article-pdf/479/1/900/25139601/sty1454.pdf
23. R.C. Pantig, Apparent and emergent dark matter around a Schwarzschild black hole. Phys. Dark Univ. **45**, 101550 (2024). https://doi.org/10.1016/j.dark.2024.101550. arXiv:2405.07531 [gr-qc]
24. V. Perlick, O.Y. Tsupko, Calculating black hole shadows: review of analytical studies. Phys. Rep. **947**, 1–39 (2022). https://doi.org/10.1016/j.physrep.2021.10.004. arXiv:2105.07101 [gr-qc]
25. G.W. Gibbons, M.C. Werner, Applications of the Gauss–Bonnet theorem to gravitational lensing. Class. Quantum Gravity **25**, 235009 (2008). https://doi.org/10.1088/0264-9381/25/23/235009. arXiv:0807.0854 [gr-qc]
26. H. Waseem, N.J.L.S. Lobos, A. Övgün, R.C. Pantig, Analyzing deflection angles and photon sphere dynamics of magnetically charged black holes in nonlinear electrodynamic. Eur. Phys. J. C **85**(6), 629 (2025). https://doi.org/10.1140/epjc/s10052-025-14373-w. arXiv:2502.04044 [gr-qc]
27. F. Ahmed, I. Sakalli, A. Al-Badawi.: Gravitational lensing phenomena of Ellis- Bronnikov-Morris-Thorne wormhole with global monopole and cosmic string. Phys. Lett. B **864**, 139448 (2025). https://doi.org/10.1016/j.physletb.2025.139448. arXiv:2503.00082 [gr-qc]
28. E. Sucu, I. Sakalli.: Exploring Lorentz-violating effects of Kalb-Ramond field on charged black hole thermodynamics and photon dynamics. Phys. Rev. D **111**(6), 064049 (2025). https://doi.org/10.1103/PhysRevD.111.064049
29. S. Mandal, Weak deflection angle, Hawking radiation, greybody bound and shadow cast for static black hole in the framework of f(R) gravity. Phys. Dark Univ. **42**, 101374 (2023). https://doi.org/10.1016/j.dark.2023.101374. arXiv:2309.16461 [gr-qc]
30. D. Kastor, S. Ray, J. Traschen, Enthalpy and the mechanics of AdS black holes. Class. Quantum Gravity **26**, 195011 (2009). https://doi.org/10.1088/0264-9381/26/19/195011. arXiv:0904.2765 [hep-th]
31. D. Kastor, S. Ray, J. Traschen, Black hole enthalpy and scalar fields. Class. Quantum Gravity **36**(2), 024002 (2019). https://doi.org/10.1088/1361-6382/aaf663. arXiv:1807.09801 [gr-qc]
32. D.V. Singh, S. Upadhyay, Y. Myrzakulov, K. Myrzakulov, B. Singh, M. Kumar, Thermodynamic behavior and phase transitions of black holes with a cloud of strings and perfect fluid dark matter. Nucl. Phys. B **1016**, 116915 (2025). https://doi.org/10.1016/j.nuclphysb.2025.116915
33. A. Benkrane, D.E. Zenkhri, Impact of dark matter halo on black hole: thermodynamical properties and photons motion. Nucl. Phys. B **1018**, 117069 (2025). https://doi.org/10.1016/j.nuclphysb.2025.117069